Investigation of possible free-radical scavengers and metrics for radiation damage in protein cryocrystallography†

James Murray and Elspeth Garman*

Laboratory of Molecular Biophysics, Department of Biochemistry, Oxford University, Rex Richards Building, South Parks Road, Oxford OX1 3QU, UK.
E-mail: elspeth@biop.ox.ac.uk

The introduction of highly intense wiggler and undulator beamlines has reintroduced the problem of X-ray radiation damage in protein crystals even at cryogenic temperatures. Several metrics for monitoring radiation damage are considered and unit-cell volume expansion is systematically investigated using crystals of three different types, but it is found to be too variable to be a useful metric. Radical scavengers of secondary radiation damage are investigated as possible mitigating agents. Styrene is found to be ineffective. A method of spectroscopically measuring the radiation damage with a microspectrophotometer was used and, in conjunction with crystallographic data, provided tentative but suggestive evidence for the efficacy of ascorbate as a free-radical scavenging agent in cryocooled hen egg-white lysozyme crystals.

Keywords: X-ray diffraction; radiation damage; free-radical scavengers; protein crystallography.

1. Introduction

Until the development of cryocrystallographic techniques, the problem of radiation damage during X-ray data collection was severe, and several crystals were usually required to obtain a complete data set. The widespread use of cryocrystallographic techniques now enables entire data sets to be collected from single crystals. Henderson (1990) has calculated that the lifetime of cryocooled crystals should be approximately five years on a rotating-anode source and one day on a wiggler-fed synchrotron beamline.

The introduction of intense multipole wiggler and undulator beamlines on second- and third-generation synchrotron sources has reintroduced the problem of radiation damage even in cryocooled crystals. Thus, once again, more than one crystal is sometimes required to obtain a complete data set.

For a well diffracting crystal, the X-ray detectors currently available do not have sufficient dynamic range to allow the full beam flux to be used without overloading low-resolution reflections unless very short exposure times are used (less than 1 s). These short exposure times result in unacceptable systematic and random errors in the data due to goniometer motor imperfections and temporal beam microstructure. There is thus a lower limit on the exposure time that can reasonably be used. To overcome these problems, third-generation undulator protein crystallography beams are frequently attenuated, thus not utilizing the full potential of the available X-ray flux.

For multiple anomalous dispersion (MAD) experiments, which require several isomorphous data sets of high quality, the deterioration of the cryocooled crystal during the experiment can cause the structure determination to fail. In fact, radiation damage is thought to be the underlying cause of most unsuccessful MAD experiments on the structural biology beamlines at the European Synchrotron Radiation Facility (ESRF) (McSweeney, 2001).

In addition to general damage effects such as increased mosaicity, $R_{\rm sym}$, Wilson B factors, and loss of resolution, specific structural damage has also been shown to occur in proteins. This includes the breaking of disulfide bonds and the loss of carboxylate groups from aspartate and glutamate residues (Weik *et al.*, 2000; Burmeister, 2000; Ravelli & McSweeney, 2000). The occurrence of such specific structural damage may be indistinguishable from that caused by mechanistic reactions (van Thor *et al.*, 2002), leading us to question the validity of our biological results from solved macromolecular structures.

An X-ray photon impinging on a crystal may pass through, be diffracted by or be absorbed by the crystal. Primary radiation-damage events occur when an X-ray photon interacts inelastically with an atomic electron within the crystal and energy is thus absorbed. These primary events result in the creation of radical species (including electrons) within the crystal, which then react further to produce cascades of secondary radicals. Direct events are those in which the radical species are produced from constituents of the protein molecule; events where radicals are formed by interactions with non-protein atoms are known as indirect. Thus both primary and secondary radicals can result in direct and indirect events, as illustrated in Fig. 1.

Very little can be done to prevent primary radiation damage, although Arndt (1984) has suggested that, for the collection of X-ray data with maximal diffracted intensity for minimal energy deposited in the crystal, the incident X-ray wavelength should be as short as possible. This has been investigated for a white beam (Gonzales & Nave, 1994), but detailed experimental verification with a monochromatic beam has yet to be obtained.

The dose rate may also be a factor relevant to the damage process; high-intensity short-exposure experiments may allow data to be collected before secondary damage becomes too severe. Conversely, high-intensity radiation may cause damage to two neighbouring sites in the crystal, which may then interact. These may have a much reduced probability of relaxing back to a predamaged state compared with that for a single damage site. This would result in a non-linear relationship between dose and damage. The effect of dose rate on radiation damage has yet to be fully tested. Some interesting experiments in this area have recently been performed (McSweeney, 2001; Sliz *et al.*, 2002) but no consensus has yet emerged.

Although it may be difficult to limit primary radiation damage, parameters that may affect the rate of secondary damage are more amenable to modification by experimenters. It may be possible to decrease the level of secondary damage by manipulating the physical and chemical environment of the crystal to one in which damage is less favoured; for example, by lowering the cryotemperature using helium cryostats to hold the crystal below the standard value of 100 K (Hanson *et al.*, 2001, 2002) or by using an alternative cryoprotectant agent. The effect of different cryoprotectant agents on the rate of production of secondary radicals has yet to be investigated. Glycerol is frequently used at very high concentrations and its impact on the damage is unknown, but it may be influential (O'Neill, 2001). Another possibility for damage reduction is that radical scavengers could be incorporated into the crystal lattice by soaking or cocrystallization so that the interaction of radicals with the protein is decreased. In order to investigate these various options systematically, it would be advantageous to know the relative proportions of primary and secondary damage, so that we can judge how much potential there is for the secondary effects of damage to be mitigated.

† Presented at the 'Second International Workshop on Radiation Damage to Crystalline Biological Samples' held at Advanced Photon Source, Chicago, USA, in December 2001.

This ratio is as yet unknown, and it is not clear how it could be measured.

At room temperature, protein crystals exposed to X-rays suffer continuing damage after the exposure has finished. This is because radicals created by the incident radiation are mobile within the crystal lattice and react with it, producing cascades of secondary radicals. Thus, the damage is both dose and time dependent. Macromolecular crystals are now routinely cooled to around 100 K (Garman & Schneider, 1997; Rodgers, 1997) to reduce the mobility of radiation-induced free radicals. The observation of specific structural damage to the protein even at this temperature indicates that some radical species, in particular electrons, are still mobile (Jones *et al.*, 1987). Radical scavengers may be able to interact with these species, reducing both their mobility and their reactivity, and also may be able to facilitate the neutralization of immobile ionized groups formed in primary or secondary interactions. The protein in the crystal would thus be protected from secondary direct damage events, resulting in an extension of the crystal lifetime. Radical scavengers are known to prevent damage to deoxyribonucleic acid (DNA) in solution (*e.g.* Fulford *et al.*, 2001) and to protein crystals at room temperature (Zaloga & Sarma, 1974).

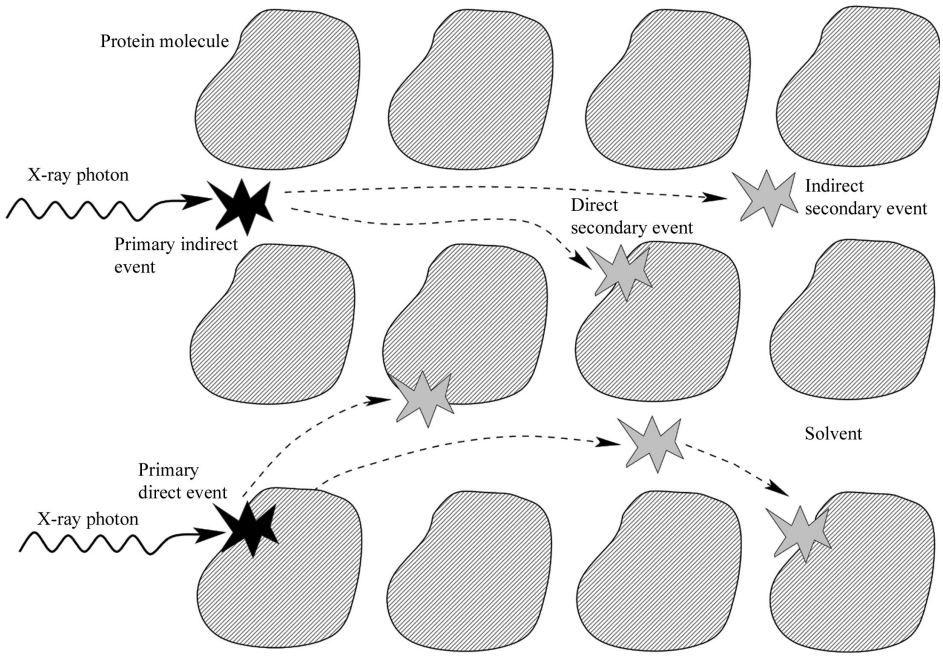

Figure 1
Primary, secondary, direct and indirect radiation-damage events in a protein crystal. The incoming X-ray photons cause primary damage events, represented by darker stars. The paths of secondary radicals are shown by dotted arrows, and the damage events they induce are represented by lighter stars. Direct events occur on the protein molecules, and indirect events occur in the solvent region.

In this paper, we present data on two different but related areas: a preliminary investigation of radical scavengers and a systematic evaluation of unit-cell volume change as a radiation-damage 'metric'. The latter investigation was prompted by the need of ourselves and other radiation-damage investigators for a generally reliable radiation-damage metric. Eventually a metric such as this could be used online as a routine tool to monitor the state of crystals during data collection.

2. Unit-cell volume as a possible radiation-damage metric

2.1. Introduction

The extensive data processing necessary for the investigation of the effects of scavengers (see §3) and the need to produce many refined electron-density maps prompted experiments to test a simple 'metric' of radiation damage.

However, the quantitation of the amount of radiation damage suffered by a macromolecular crystal is far from straightforward. Various properties of the diffraction data might be useful as radiation-damage metrics, such as the changes as data collection proceeds in Wilson B factors, mosaicity, $R_{\rm sym}$ or an appropriately weighted merging statistic, such as the pooled coefficient of variance (PCV) (Diederichs & Karplus, 1997), the average $\langle I \rangle/\sigma_I$ in the outer resolution shell, the intensity of a single reflection measured over time or the specific damage seen in electron-density maps.

These quantities all have drawbacks as metrics in that either they require the data to be reduced and scaled before they can be evaluated, or they vary if there is anisotropy in the crystal and so change over the φ range of the data collection. It is also known (Ravelli & McSweeney, 2000) that specific damage starts to occur before the diffraction pattern is compromised. The production of electron-density maps requires the structure to be solved and refined before specific damage can be seen. Refined electron-density maps are time-consuming to produce, and this increases the difficulty of comprehensive and statistically significant radiation-damage experiments.

Another possible metric suggested by Ravelli & McSweeney (2000) is the unit-cell volume, which is known to expand with increasing radiation dose. The unit cell also expands with increasing temperature (Weik *et al.*, 2001), but recent theoretical analyses (Nicholson *et al.*, 2001; Kuzay *et al.*, 2001) show that, under the regime of a small crystal mounted in a loop bathed in a stream of nitrogen gas at 100 K, crystal heating by an intense synchrotron beam should normally be under 10 K. Unit-cell expansion due to beam heating is thus expected to be low compared with the observed unit-cell expansion caused by incident radiation. We therefore undertook a systematic investigation of the change in unit-cell volume as a possible radiation-damage metric.

2.2. Experimental details

The expansion in cell volume with radiation dose was measured for four crystals each of horse-spleen light-chain holoferritin, apoferritin and influenza N9 neuraminidase. These crystals were chosen for their different compositions but similar unit-cell parameters and symmetry. All systems are cubic; the ferritin crystals are in space group $F432$ with $a = b = c \simeq 181$ Å and the neuraminidase crystals are in $I432$ with $a = b = c \simeq 181$ Å. The cubic symmetry was important for the reliable extraction of the unit cell, since only a single cell-edge length required fitting, and so it was well determined for all values of φ.

2.2.1. Crystallization. Horse-spleen holoferritin and apoferritin were obtained from Sigma and were used with no further purification. They were crystallized by hanging-drop vapour diffusion from a 1:1 mixture of 50 mg ml^{-1} ferritin, 0.1 M sodium chloride solution and 0.8 M ammonium sulfate, 10 mM cadmium sulfate with 25% glycerol v/v. The mother-liquor solution was sufficiently cryoprotective for the

crystals to be flash cooled directly from the drop into a 100 K nitrogen gas stream.

N9 neuraminidase was purified and crystallized as described previously (Laver *et al.*, 1984). Crystals were grown by hanging-drop vapour diffusion from a mother liquor of 1.7 *M* potassium phosphate. A single large crystal was selected and four smaller crystal were obtained from it by dissection with an acupuncture needle. These crystals were serially cryoprotected *in situ* (Garman, 1999) up to a concentration of 40% glycerol *v*/*v* in 10% steps over a total of three minutes and then flash cooled in a 100 K nitrogen gas stream as required.

2.2.2. Data collection and processing. Crystals were selected to be as near as possible to the same size: around 80 µm in their linear dimensions. Calculations with *RADDOSETST* (Ravelli, 2000) for an N9 crystal show that, for cubic crystals, increasing the edge from 50 µm to 100 µm reduces the specific (*i.e.* per unit mass) absorbed dose by 1%, and for crystals of edge 50 µm to 1000 µm the corresponding change is 8%. Therefore, small variations in crystal size do not contribute significantly to variations in specific absorbed dose. Note that although the total absorbed dose increases with crystal size, the specific absorbed dose decreases.

The unattenuated beam on ID14-EH4 at the ESRF with wavelength 0.9393 Å and slits set to 200 × 200 µm was used. For all crystals, the crystal-to-detector distance was 250 mm and the resolution was cut at 2.7 Å, which corresponded to the largest circle that could be completely inscribed on the square CCD detector. Each small crystal of holoferritin, apoferritin and N9 neuraminidase was subjected to nine repeated sweeps of 10° in φ, each sweep consisting of ten images of 1 s exposure and $\Delta\varphi$ of 1° per image. The incident dose per image was monitored using the beamline ion chamber and was approximately constant for all the images. The calculation described above shows that the absorbed dose was effectively constant within each protein type as the crystals were all of very similar size. The total absorbed doses were estimated as 3×10^6 Gy, 7×10^5 Gy and 7×10^5 Gy for holoferritin, apoferritin and N9 neuraminidase, respectively.

The initial image of the first set of images for each crystal was used for indexing (Kabsch, 1988), and then an overall unit cell for each set was refined from this using the *Mosflm* 'post-refinement' procedure (Leslie, 1992). An attempt to quantify the error in the cell-length refinement was made by also refining a cell length from the first five and the last five images in each ten-image φ scan. This was unsatisfactory because the cell changed between the first five and last five images. It should be possible to obtain a better estimate of the errors by extracting independent estimates of the *a*, *b* and *c* parameters through refinement of the cell lengths in an orthorhombic space group. This was attempted, but the refinement was found to be unstable over the small φ range of the scan.

The data from each φ scan were also integrated in *Mosflm* and scaled using programs of the *CCP*4 suite (Collaborative Computational Project, Number 4, 1994). The same scripts were used for all 108 φ scans (with minor modifications for space group). For one of the 12 crystals, these processing parameters did not produce scaled data for five of the nine φ scans. The reason for this has not been investigated in detail, but could be due to the need for fine-tuning of the scaling of each individual φ scan.

2.3. Results of the unit-cell expansion experiments

The results of these experiments (see Fig. 2) show that the relative unit-cell volume expansion is linear with dose but that the rate of expansion is variable between crystals of the same protein. The unit-cell volume expansions observed in these crystals range from 0.0% to 1.1% for apoferritin, −0.7% to 5.0% for holoferritin and 0.5% to 1.2% for N9 neuraminidase. The errors (as estimated, not plotted) were small compared with the relative differences between crystals. Note that for holoferrin crystal 3 (Fig. 2*b*) the unit-cell volume actually decreases: so far we have no reasonable explanation for this

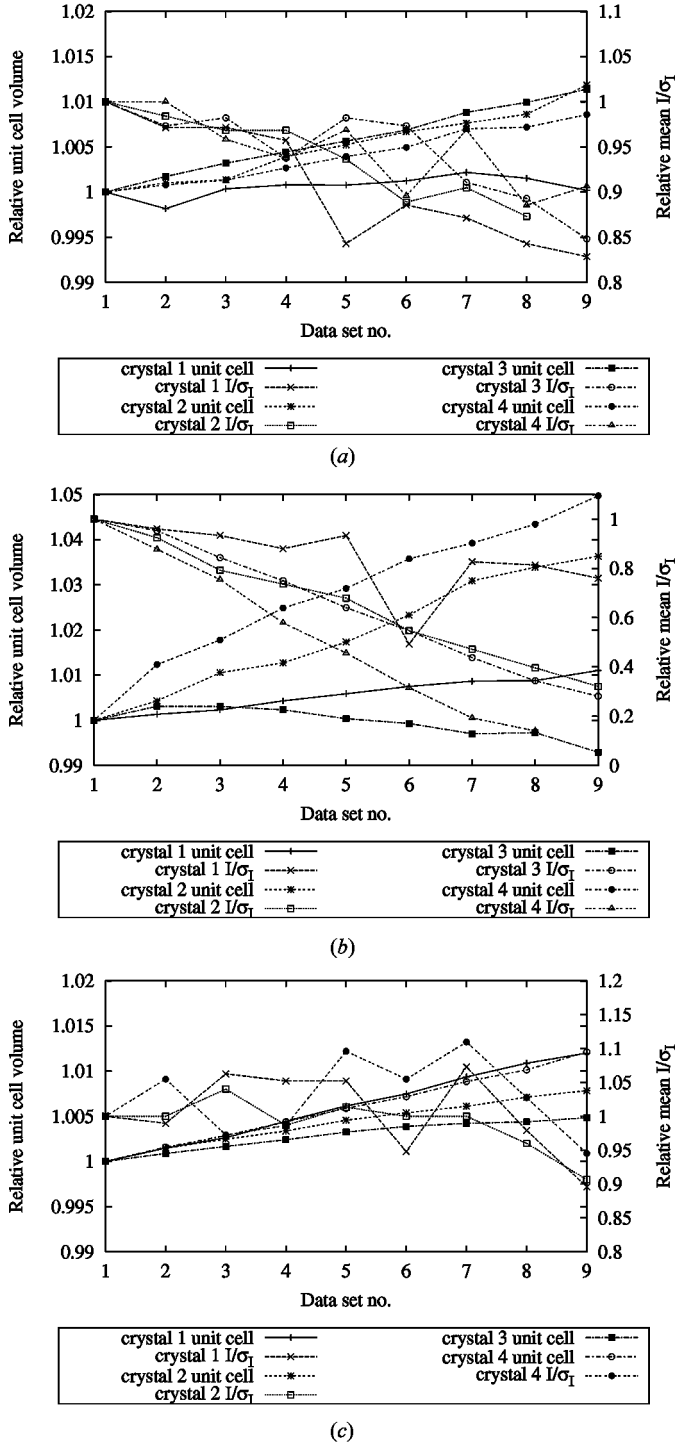

Figure 2
Graphs to show the relative unit-cell volumes (left *y* axis) and I/σ_I (right *y* axis) of crystals with increasing radiation dose for four crystals each of three different types. The cumulative absorbed dose at each data point is proportional to the data set number. (*a*) Apoferritin. (*b*) Holoferritin. (*c*) N9 neuraminidase.

observation. This reinforces our conclusion that the change in unit cell with dose is highly variable for different crystals of the same protein.

The unit-cell volumes of the holoferritin crystals show the largest overall expansion, as is expected, since owing to their high iron content they have the largest primary absorption. It is also possible that crystal heating may play a role in this effect (Ravelli *et al.*, 2002).

For tetragonal hen egg-white lysozyme (HEWL) crystals, it has been reported (Teng & Moffat, 2000) that above a certain dose the unit-cell volume expansion becomes non-linear; this non-linear region was not observed here. As can be seen from Fig. 2, the change in cell volume is a more stable parameter with radiation dose than I/σ_I, which predictably shows a general trend to decrease in value, but shows a significant scatter about the average decrease indicating that it would not be a reliable radiation-damage metric.

2.4. Discussion of unit-cell expansion

In these experiments, small changes in unit-cell volume are being measured: 5% expansion of the cell volume in the most extreme case (holoferritin crystal 4). However, a more typical value is ∼1% of the cell volume, corresponding to a difference in linear cell dimension of 0.6 Å (in 181 Å), which is of the same order as the absolute differences in cell volume noted between different flash-cooled crystals of the same type. The extracted cell lengths are strongly dependent on the processing protocol used and the way in which the data-reduction package is applied (Grimston, 2001). It is important that the parameters of the positional refinement are carefully controlled, since errors in one parameter can compensate for errors in another. This leads to an acceptable spot prediction and integration but inconsistent unit-cell parameters between φ scans. The unit-cell expansion is less well defined on systems that have symmetries lower than cubic and the φ range over which the cell lengths are extracted then becomes important.

The systems chosen here are particularly favourable for systematic measurements, having high cubic symmetry and large unit cells. This results in many spots per image, and it is not clear whether small changes in unit-cell dimensions could be measured accurately enough for systems with lower symmetry.

The rate of unit-cell volume increase showed a large variation within crystals of the same type after the same radiation dose. As mentioned previously, this variation is unlikely to be due to differences in absorbed dose between different crystals, as calculations show that for crystals of roughly the same size the difference in specific absorbed dose is small (±0.5% for the range of crystal sizes in these experiments).

The mechanism by which the unit cell expands with radiation dose is not understood: it is not even known whether it is a primary or secondary damage effect. We have observed that the expansion is highly variable between similar-sized crystals of the same protein grown under identical conditions and for similar-sized fragments of the same protein crystal, even though the incident dose is constant to within 10%.

We conclude that, although observable, the cell-expansion effect is small. It is not sufficiently reproducible for a given protein to allow an expansion criterion to be defined above which the radiation damage could be considered significant. However, it should be noted that crystals for which the unit-cell expansion is small during the course of the data collection will give more isomorphous, and hence better, data.

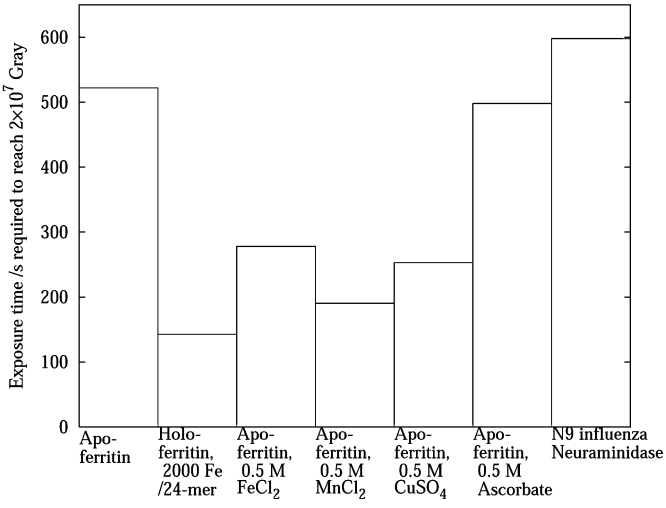

Figure 3
Histogram to show the estimated time for the Henderson absorption limit of 2×10^7 Gy to be reached for various protein crystals of the same size containing different scavengers under typical unattenuated conditions at beamline ID14-EH4 at the ESRF, Grenoble. The absorbed dose calculations were performed with the program *RADDOSETST* (Ravelli, 2000).

3. Scavengers

Many potential scavengers for protein crystals have been mentioned in the literature, although very few have been tested experimentally. Suggested scavengers include ethanol, thiourea (Blundell & Johnson, 1976), ascorbate, cysteine, glutathione, *t*-butanol, *N*-2-hydroxyethylpiperazine-*N*′-2-ethanesulfonic acid (HEPES), tris(hydroxymethyl)aminoethane (Tris), glucose, ethylene glycol and styrene. Some of the putative scavengers also have the advantage that they are known cryoprotectant agents. Scavengers are widely used in electron spin resonance (ESR) spectroscopy as spin traps; for example 5,5-dimethylpyroline-*N*-oxide (DPMO) and 2,2,6,6-tetramethyl-4-piperidone (TEMP). These react with short-lived radical species to form more stable radical adducts, which are then detectable by the ESR instrument. Such spin traps may have applications in crystallography as they reduce the reactivity of radicals, but they have so far not been investigated.

Transition-metal compounds can act as acceptors for free electrons and so could be used as radical scavengers in protein crystals. However, the presence of such metal ions in the concentrations required for effective scavenging would probably increase the absorbed radiation dose of the crystal to an unacceptable level. For example, ferritin can hold up to 4500 iron atoms per 24-mer, a concentration of 5 *M* iron in the crystal. Holoferritin crystals are known to be very sensitive to radiation damage, and no holoferritin X-ray crystal structure has yet been published.

To decide whether metal compounds might be of use as scavengers in protein crystallography, the time taken to reach the so-called 'Henderson dose limit' (Henderson, 1990) for various compounds has been calculated. This limit was originally derived by computing the equivalent radiation dose observed to cause terminal damage to biological samples in cryoelectron microscopy. For protein crystals, a dose of 2×10^7 Gy is expected to severely compromise the diffraction pattern.

The time taken to reach this limit in an undulator-produced beam has been calculated for holoferritin, apoferritin and N9 neuraminidase with different scavengers. The absorption coefficient, μ, of the protein crystal can be calculated from its chemical composition.

The absorbed dose can then be calculated from μ and the parameters of the incident X-ray beam. The results are illustrated in Fig. 3, which shows that adding transition-metal compounds to crystals in the concentrations likely to be useful for scavenging would increase the primary absorption to a level similar to that of holoferritin. As a result of these calculations, we have decided not to investigate transition-metal scavengers further. In contrast, small organic molecules have little effect on the primary absorption and so are more likely to be useful as free-radical scavengers.

3.1. Styrene as a free-radical scavenger

Styrene and other small aromatic molecules such as methylmethacrylate and chlorostyrene have been used as scavengers in protein crystallography in the past. Researchers (Zaloga & Sarma, 1974; Sarma & Zaloga, 1975) have reported that styrene soaked into particularly radiation-sensitive immunoglobulin crystals extended the resolution from 5.5 Å to 4 Å and increased the effective crystal lifetime by a factor of ten as measured by the intensity of a single reflection at room temperature. We have investigated the use of styrene as a potential scavenger at 100 K for HEWL crystals.

3.1.1. Experimental details and results. HEWL crystals in space group $P4_32_12$ were grown by hanging-drop vapour diffusion from a 1:1 mixture of 100 mg ml^{-1} HEWL (HEWL was purchased from Sigma and used without further purification), 50 m*M* sodium acetate, pH 4.5 solution, and 30% *w*/*v* MPEG 5 K, 1.0 *M* sodium chloride, 50 m*M* sodium acetate, pH 4.7. HEWL was cocrystallized with styrene from precipitant solutions that had been overlaid with styrene, shaken vigorously and then allowed to separate for several hours to produce a saturated styrene solution. Crystals were cryoprotected for a few minutes in the mother liquor made up with 10% glycerol *v*/*v*, before being flash cooled in a loop (Teng, 1990) in a 100 K nitrogen gas stream.

Data were collected from three crystals each of styrene-cocrystallized and native HEWL crystals using identical beam conditions at ID14-EH4, ESRF, Grenoble, set at a wavelength of 0.9795 Å. Each crystal was subjected to nine repeated sweeps of 10° in φ, each sweep consisting of ten images of 1 s exposure and $\Delta\varphi$ of 1°, with a beam attenuated tenfold. Between successive sweeps in φ, the crystal was exposed for 30 s to the unattenuated beam. For one each of the styrene-containing and native crystals, two full data sets of resolution 1.3 Å (ADSC Quantum 4 CCD, detector distance 100 mm) were recorded, one before and one after the sweeps in φ. For these data sets, the beam was also attenuated by a factor of ten in order to minimize structural damage during the course of collection. The total absorbed dose for each crystal was estimated to be approximately 1×10^7 Gy.

All doses were estimated from the ion-chamber reading on the beamline, which was calibrated with a photodiode, assuming a linear relationship between ion-chamber current and photons. The absorbed dose was then estimated from the number of incident photons, the crystal size and composition, and the incident wavelength using the program *RADDOSETST* (Ravelli, 2000). Given the many inaccuracies inherent in this process, the doses should only be considered accurate to within an order of magnitude. We are actively working on a better calibration of incident dose.

Refined structures were produced from the four data sets. Crystal data such as expansion of unit-cell volume and reduction in diffracted intensity were analysed from the styrene-cocrystallized and native crystals. No significant differences were noted between the native and styrene-containing crystals, as indicated by $R_{\rm merge}$, I/σ_I and the unit-cell volume expansion (data not shown). The electron-density maps calculated from the refined structures were also analysed and no difference in specific structural damage was observed (data not shown).

The results of these experiments imply that under the conditions used the scavenger had no detectable effect. In addition, styrene is difficult to work with since it is toxic, volatile and only very sparingly soluble in water. It is thus not a promising tool for mitigation of radiation damage in protein crystals at cryotemperatures.

3.2. Ascorbate as a free-radical scavenger

The results presented in §2 show that unit-cell expansion is not a reliable metric by which to judge the effect of potential scavengers on crystal lifetime, so a new strategy was employed to investigate the effects of a second scavenger: ascorbate. As well as collecting a complete data set on each φ sweep so that electron-density maps could be calculated and compared for each sweep, an offline microspectrophotometer was used to monitor changes in the absorption spectrum of the crystal.

3.2.1. Experimental details. HEWL was purchased from Sigma and was used without further purification. Tetragonal crystals in space group $P4_32_12$ were grown by hanging-drop vapour diffusion from a 1:1 mixture of 50 mg ml^{-1} HEWL in 200 m*M* sodium acetate, pH 4.7, and 3–7% sodium chloride, 200 m*M* sodium acetate, pH 4.7, according to the method of Drenth (1999). Crystals were also grown in the presence of ascorbate by adding 1.0 *M* sodium ascorbate to the precipitant solution. This corresponded to approximately nine ascorbate molecules in the crystal per HEWL molecule, based on a concentration of 59 m*M* HEWL in the tetragonal crystals grown.

Crystals were cryoprotected by soaking them for less than a minute in the precipitant solution diluted to give 20% *v*/*v* glycerol.

Cryoprotected HEWL crystals were mounted in rayon loops and flash cooled in a 100 K nitrogen gas stream. Successive data sets were taken from two lysozyme crystals: one with and one without ascorbate. The unattenuated beam of ID14-EH4 at the ESRF, set at a wavelength of 0.9390 Å and slit settings of 150 × 30 µm, was used.

For each crystal, the six successive data sets consisted of 135 images of $\Delta\varphi = 0.5°$ and 0.5 s exposure per image. The crystal-to-detector distance was 100 mm; the data were processed to a resolution of 1.3 Å.

We present here an analysis based on the first and last data set from each crystal. The total absorbed dose for each crystal was estimated to be 1×10^7 Gy.

Each data set was reduced and scaled using programs of the *CCP*4 suite (Collaborative Computational Project, Number 4, 1994). A lysozyme structure, 193L (Vaney *et al.*, 1995), stripped of non-protein atoms was used as a starting model. The structures were subject to 30 cycles of rigid-body refinement in *REFMAC* (Murshudov *et al.*, 1997) and then 30 cycles of restrained refinement of all atoms. Tables 1 and 2 show the results of the data processing and refinement for the first and last data set of each crystal. It will be noted that although the quality of the data from the crystal grown in the presence of ascorbate is reasonable, that from the native HEWL crystal is poor, having a high value of the PCV. However, for the purposes of the comparisons necessary for this particular investigation, the quality is adequate. To facilitate comparisons between the crystals, no solvent atoms were added during the refinement, and this helps to explain the rather high *R* factors in Table 2.

The effect of the presence of ascorbate on the radiation sensitivity of the HEWL crystals was further investigated using an offline microspectrophotometer equipped with a cryostat and goniostat and operating with a deuterium light source (Bourgeois *et al.*, 2002).

Table 1
Data-reduction statistics for the first and sixth data sets from the native and the ascorbate-containing tetragonal HEWL crystals.

The figures in parentheses refer to the highest-resolution shell. PCV is defined as $\{\sum_h[(n_h-1)^{-1}\sum_i^{n_h}(I_{(h,i)}-\hat{I}_h)^2]^{1/2}\}/\sum_h\hat{I}_h$ where $\hat{I}_h = n_h{}^{-1}\sum_i^{n_h} I_{(h,i)}$.

	Data set			
	Native #1	Native #6	Ascorbate #1	Ascorbate #6
Unit cell (Å)	$a = b = 78.23$, $c = 36.94$	$a = b = 78.23$, $c = 36.94$	$a = b = 77.26$, $c = 37.22$	$a = b = 77.27$, $c = 37.22$
Resolution (Å)	39.2–1.3 (1.37–1.30)	39.2–1.3 (1.37–1.30)	38.6–1.3 (1.37–1.30)	55.0–1.3 (1.37–1.30)
No. of unique reflections	29181	29241	28290	28371
Redundancy	4.1 (4.0)	4.2 (4.1)	5.0 (5.0)	5.0 (5.0)
$(I)/\sigma_I$	13.0 (3.7)	13.1 (1.4)	22.5 (6.0)	25.1 (5.4)
Completeness (%)	97.0 (97.0)	98.5 (98.5)	99.1 (98.8)	99.2 (99.4)
PCV	0.11 (0.32)	0.14 (1.31)	0.06 (0.25)	0.06 (0.26)
Wilson B factor	12.5	15.4	13.4	13.2
Absolute scale factor	0.41	1.1	1.3	2.6

Spectra were recorded with an integration time of 100 ms, and on average ten such spectra were recorded. The protein crystal was located in the loop by the presence of a large absorption maximum at 280 nm.

Absorption spectra were collected from unexposed crystals with and without ascorbate as well as from X-ray-exposed crystals. Controls consisting of loops with mother liquor only, both with and without ascorbate present, and unexposed and exposed to X-rays, were also collected. For the X-ray exposures, the unattenuated ID14-EH4 beam through slits of 120×30 µm and at a wavelength of 0.9390 Å was incident on the cryocooled samples for 300 s over a φ range of 300°. The absorbed radiation dose was estimated to be 0.8×10^7 Gy. The exposed samples were transferred to liquid nitrogen at 77 K and then remounted on the microspectrophotometer, thus remaining below 100 K at all times. For the X-ray-exposed crystals, spectra were measured at 30 min intervals for 90 min.

3.2.2. Results. The 'classic' sites of specific radiation damage as seen in electron-density maps are the loss and breakage of disulfide bonds and the ablation of carboxylate groups from aspartate and glutamate residues. Electron-density maps were thus calculated to examine sites of known specific structural damage. All four disulfide bonds in HEWL were inspected and one of these, Cys76—Cys94, is illustrated in Fig. 4.

In the native crystal, this particular disulfide bond is already damaged even after one data set, whereas the crystal grown in the presence of ascorbate shows no sign of degradation at this position. Moreover, it can be clearly seen that the increase in negative difference density with radiation dose for the native crystal is greater than that for the crystal grown in the presence of ascorbate, for which no difference density can be seen at the -2.5σ level displayed in Fig. 4. For the Cys6—Cys127 disulfide bond, which is known to be the most radiation sensitive of the HEWL disulfide bonds (Ravelli & McSweeney, 2000), the effect was very similar. No ascorbate was visible in the difference-density maps for the crystal grown in the presence of ascorbate.

The relative increase in B factors (see Table 2) for cysteine residues was 41% in the native crystal compared with a 1% decrease in the ascorbate crystal. The native crystal had an increase in B factor for all atoms of 33%, compared with a decrease of 1% in the ascorbate-soaked crystal; thus, for the native crystal, the B-factor increase for the cysteine residues was greater than that for the protein as a whole. This is mirrored by the behaviour of the Wilson B factors, shown in Table 1. The Wilson B of the native crystal increases by 23% and the absolute scale factor increases by a factor of three during the course of the six data sets, whereas the Wilson B of the ascorbate crystal marginally decreases and the absolute scale factor increases by only a factor of two. These values indicate that although scattering power is being lost from the crystals as the data collection proceeds, what remains in the ascorbate-soaked crystal is still as ordered as at the

Table 2
Refinement statistics for the first and sixth data sets from the native and the ascorbate-containing HEWL crystals.

	Data set			
	Native #1	Native #6	Ascorbate #1	Ascorbate #6
$R_{\rm factor}$ (%)	28.7	29.9	26.1	25.9
$R_{\rm free}$ (%)	31.1	32.5	28.8	29.6
Average B factor (Å^2)	16.1	21.4	17.7	17.5
Average cysteine B factor (Å^2)	12.8	18.0	16.4	16.2

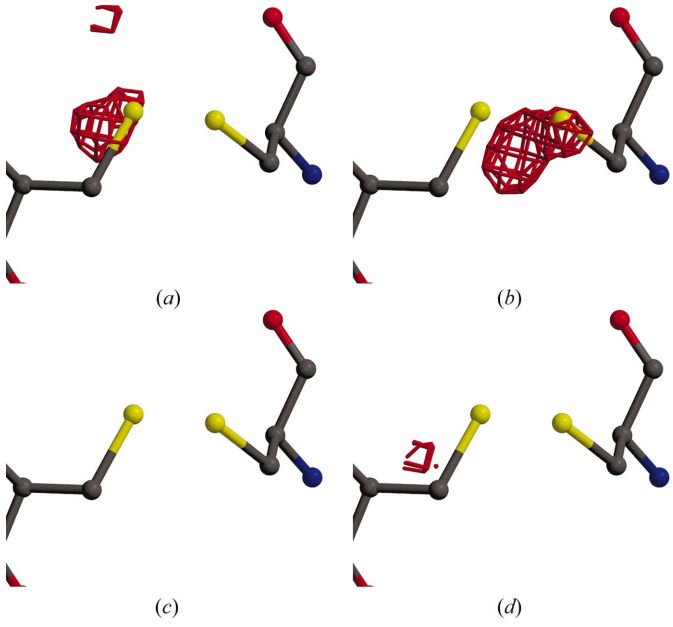

Figure 4
Electron-density maps of the Cys76—Cys94 disulfide bond in HEWL crystals. The F_o–F_c maps are σ_A weighted and are contoured at -2.5σ: (*a*) is calculated from the first data set from the native HEWL crystal, (*b*) is calculated from the sixth data set from the native crystal, (*c*) is calculated from the first data set from the crystal grown in the presence of ascorbate and (*d*) is calculated from the sixth data set from the crystal grown in the presence of ascorbate. The figure was produced using *MOLSCRIPT* (Kraulis, 1991), *CONSCRIPT* (Lawrence & Bourke, 2000) and *RASTER3D* (Merritt & Bacon, 1997).

start of the experiment, while the native crystal has lost scattering power and order.

The absorption spectra for loop-mounted crystals and solvent are displayed in Figs. 5 and 6. The spectra show that the X-ray-exposed crystals without ascorbate present have an absorption maximum at 400 nm. This maximum is not present in the unexposed crystals and decays with time. The control experiments performed on the crystal mother liquor gave no absorption maximum at 400 nm, indicating that this maximum is indeed caused by the presence of the protein. However, crystals soaked in ascorbate do not show this maximum but have an absorption maximum at 350 nm, which is also present in the spectrum of the ascorbate-containing solvent and does not decay with time. Therefore, we attribute this 350 nm maximum to the presence of ascorbate, although we cannot unambiguously assign the peak to a particular species.

The maximum at 400 nm observed in the spectrum from the X-ray-exposed native HEWL crystal is thought to be from a disulfide radical species (Favaudon *et al.*, 1990; Weik *et al.*, 2002). The X-ray-exposed crystal grown in the presence of ascorbate did not show this maximum, which implies that the ascorbate is directly or indirectly scavenging these radicals.

4. Discussion of ascorbate as a scavenger

The smaller differential relative changes in *B* factor and the improved electron-density difference maps for the ascorbate HEWL cocrystal, compared with those from the native HEWL crystal, imply that the ascorbate cocrystal is less sensitive to X-ray radiation than the native crystal.

The absorption maximum at 400 nm present in the native X-ray-exposed HEWL crystal is thought to be due to a disulfide radical species. As noted above, this maximum is not present in the spectrum from the ascorbate-soaked crystal, indicating that the ascorbate is directly or indirectly scavenging these radicals.

These results must be replicated with more HEWL crystals and for other proteins to give this finding statistical significance, since only a single crystal of each type was used for the crystallographic data collection. However, the findings presented here from the crystallographic and spectroscopic data give hope that scavengers might be used to mitigate radiation damage in protein crystals at cryogenic temperatures.

An additional factor yet to be investigated is the impact of glycerol as a cryoprotectant. This is present at very high concentrations and may have an effect, positive or negative, on the radiation-damage process. It is already known that glycerol accelerates photoreduction of cryocooled protein crystals by aiding the transfer of electrons to metal centres, as measured by extended X-ray-absorption fine-structure spectroscopy (EXAFS) (Hedman, 2001).

The mechanism by which the putative ascorbate scavenging acts is not yet understood. Ascorbate is known to be an OH radical scavenger (Buxton *et al.*, 1988) and an antioxidant that can restore oxidized radicals by donating an electron to them. It is possible that the ascorbate is neutralizing positively-charged protein radicals by restoring their lost electrons (O'Neill *et al.*, 2002).

The postulated mechanism by which disulfide bonds are broken by radiation (Weik *et al.*, 2002) is hard to reconcile with the damage mitigation we have observed in the presence of ascorbate. The mechanism by which the disulfide bonds are protected or repaired may not involve the direct interaction of ascorbate with the protein but may be an indirect effect involving a chain of reactions.

The hypothesis that disulfide radical species are responsible for the absorption maximum at 400 nm will be tested using a crystal of a protein or peptide with no disulfide bonds, such as horse-spleen ferritin.

5. Conclusions

We have investigated unit-cell volume increase as a possible online metric for radiation damage and concluded that it is not a reliable enough indicator to be used by protein crystallographers generally. However, if ways to mitigate radiation damage are established, it is possible that these will result in stabilization of the unit-cell volume, which will then reduce problems of non-isomorphism in MAD experiments.

A study to evaluate the potential of free-radical scavengers as mitigators of secondary radiation damage induced by intense synchrotron beams has been instigated. We have performed experiments with styrene, and, although it has been reported to act as a scavenger at room temperature, we have found no evidence for its

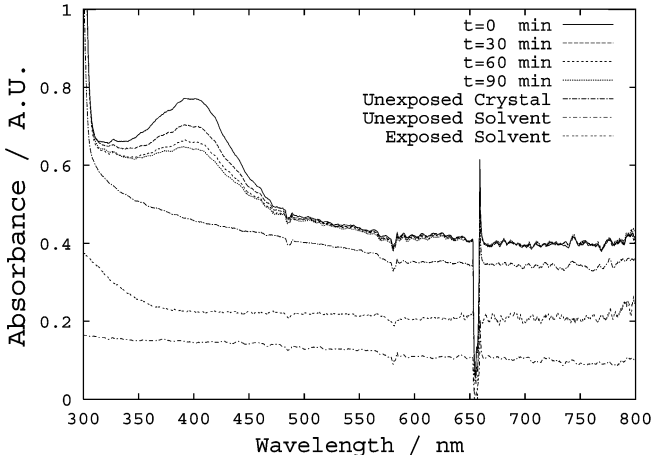

Figure 5
Absorption spectra of native HEWL crystals before and after X-ray exposure. Control data from unexposed and exposed crystal mother liquor alone are also presented.

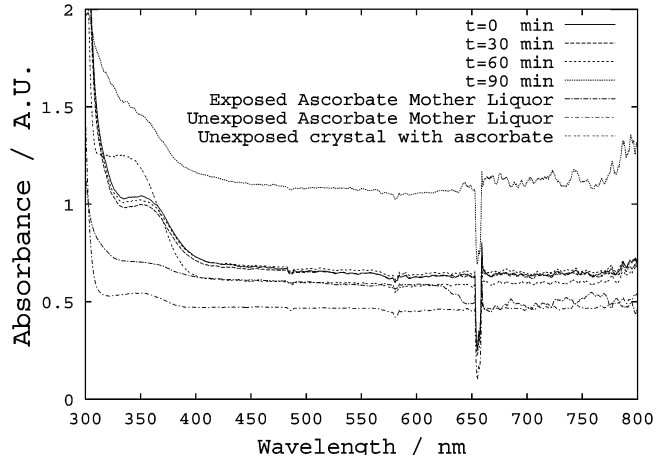

Figure 6
Absorption spectra of HEWL crystals grown in the presence of ascorbate, before and after X-ray exposure. Control data from unexposed and exposed ascorbate-containing crystal mother liquor alone are also presented.

efficacy at 100 K in HEWL crystals. However, our initial results with ascorbate and HEWL crystals show that ascorbate may have potential as a scavenger for macromolecular cryocrystallography. Its effects in the crystal were monitored spectroscopically as well as structurally and we are excited by the possibilities that this combination of techniques presents for testing a wider range of other free-radical scavengers for use in macromolecular cryocrystallography.

We gratefully acknowledge the ESRF for granting us a long-term project beamtime allocation [LS2047] and our collaborators Raimond Ravelli and Sean McSweeney on radiation-damage investigations. We thank Graeme Laver for providing the N9 neuraminidase crystals, Peter O'Neill and Jasper van Thor for helpful discussions, Dominique Bourgeois for the use of the microspectrophotometer, and Martin Weik for much help with its operation. JM has an MRC-funded studentship. Fig. 1 is after a diagram by Thomas Schneider.

References

Arndt, U. W. (1984). *J. Appl. Cryst.* **17**, 118–119.
Blundell, T. L. & Johnson, L. N. (1976). *Protein Crystallography*. New York: Academic Press.
Bourgeois, D., Vernede, X., Adam, V., Fioravanti, E. & Ursby, T. (2002). *J. Appl. Cryst.* **35**, 319–326.
Burmeister, W. P. (2000). *Acta Cryst.* D**56**, 328–341.
Buxton, G. V., Clive, L., Greenstock, W., Helman, P. & Ross, A. B. (1988). *J. Phys. Chem. Ref. Data*, **17**, 513–886.
Collaborative Computational Project, Number 4 (1994). *Acta Cryst.* D**50**, 760–763.
Diederichs, K. & Karplus, P. A. (1997). *Nature Struct. Biol.* **4**, 269–275.
Drenth, J. (1999). *Principles of Protein X-ray Crystallography*, 2nd ed. Berlin: Springer.
Favaudon, V., Tourbez, H., Houée-Levin, C. & Lhoste, J.-M. (1990). *Biochemistry*, **29**, 10978–10989.
Fulford, J., Nikjoo, H., Goodhead, D. T. & O'Neill, P. (2001). *Int. J. Radiat. Biol.* **77**, 1053–1066.
Garman, E. (1999). *Acta Cryst.* D**55**, 1641–1653.
Garman, E. F. & Schneider, T. R. (1997). *J. Appl. Cryst.* **30**, 211–237.
Grimston, J. (2001). Dissertation, University of Oxford, UK.
Hanson, B. L., Harp, J. M., Kirschbaum, K., Parrish, D. A., Timm, D. E., Howard, A., Pinkerton, A. A. & Bunick, G. J. (2001). *J. Cryst. Growth*, **232**, 536.
Hanson, B. L., Harp, J. M., Kirschbaum, K., Schall, C. A., DeWitt, K., Howard, A., Pinkerton, A. A. & Bunick, G. J. (2002). *J. Synchrotron Rad.* **9**, 375–381.
Hedman, B. (2001). Personal communication.
Henderson, R. (1990). *Proc. R. Soc. London Ser. B*, **241**, 6–8.
Jones, G. D. D., Lea, J. S., Symons, M. C. R. & Taiwo, F. A. (1987). *Nature* (*London*), **330**, 772–773.
Kabsch, W. (1988). *J. Appl. Cryst.* **21**, 67–71.
Kraulis, P. J. (1991). *J. Appl. Cryst.* **24**, 946–950.
Kuzay, T. M., Kazmierczak, M. & Hsieh, B. J. (2001). *Acta Cryst.* D**57**, 69–81.
Laver, W. G., Colman, P. M., Webster, R. G., Hinshaw, V. S. & Air, G. M. (1984). *Virology*, **137**, 314–323.
Lawrence, M. C. & Bourke, P. (2000). *J. Appl. Cryst.* **33**, 990–991.
Leslie, A. G. W. (1992). *Joint CCP4 + ESF-EAMCB Newsletter on Protein Crystallography*, No. 26.
McSweeney, S. (2001). Personnal communication.
Merritt, E. A. & Bacon, D. J. (1997). *Methods Enzymol.* **277**, 505–524.
Murshudov, G. N., Vagin, A. A. & Dodson, E. J. (1997). *Acta Cryst.* D**53**, 240–255.
Nicholson, J., Nave, C., Fayz, K., Fell, B. & Garman, E. (2001). *Nucl. Instrum. Methods Phys. Res. A*, **467**/**468**, 1380–1383.
O'Neill, P. (2001). Personal communication.
O'Neill, P., Stevens, D. & Garman, E. F. (2002). *J. Synchrotron Rad.* **9**, 329–332.
Ravelli, R. (2000). Unpublished.
Ravelli, R. B. G. & McSweeney, S. M. (2000). *Structure*, **8**, 315–328.
Ravelli, R. B. G., Theveneau, P., McSweeney, S. & Caffrey, M. (2002). *J. Synchrotron Rad.* **9**, 355–360.
Rodgers, D. W. (1997). *Methods in Enzymology*, edited by C. W. Carter Jr & R. M. Sweet, Vol. 276, pp. 183–203. London: Academic Press.
Sarma, R. & Zaloga, G. (1975). *J. Mol. Biol.* **98**, 479–484.
Sliz, P., Harrison, S. C. & Rosenbaum, G. (2002). *Acta Cryst.* A**58**, (Supplement), C72.
Teng, T.-Y. (1990). *J. Appl. Cryst.* **23**, 387–391.
Teng, T.-Y. & Moffat, K. (2000). *J. Synchrotron Rad.* **7**, 313–317.
Thor, J. J. van, Gensch, T., Hellingwerf, K. J. & Johnson, L. N. (2002). *Nature Struct. Biol.* **9**, 37–41.
Vaney, M., Maignan, S., Ries-Kautt, M. & Ducruix, A. (1995). Unpublished.
Weik, M., Bergés, J., Raves, M. L., Gros, P., McSweeney, S., Silman, I., Sussman, J. L., Houée-Levin, C. & Ravelli, R. B. G. (2002). *J. Synchrotron Rad.* **9**, 342–346.
Weik, M., Kryger, G., Schreurs, A. M. M., Bauma, B., Silman, I., Sussman, J. L., Gos, P. & Kroon, J. (2001). *Acta Cryst.* D**57**, 566–573.
Weik, M., Ravelli, R. B. G., Kryger, G., McSweeney, S., Raves, M. L., Harel, M., Gros, P., Silman, I., Kroon, J. & Sussman, J. L. (2000). *Proc. Natl Acad. Sci. USA*, **97**, 623–628.
Zaloga, G. & Sarma, R. (1974). *Nature* (*London*), **251**, 551–552.

 Received 20 February 2002 • Accepted 2 August 2002